Energies **2013**, *6*, 3353-3372; doi:10.3390/en6073353

OPEN ACCESS

energies

ISSN 1996-1073

www.mdpi.com/journal/energies

Article

A Long Gravity-Piston Corer Developed for Seafloor Gas Hydrate Coring Utilizing an *In Situ* Pressure-Retained Method

Jia-Wang Chen [1,2], Wei Fan [3,*], Brian Bingham [2], Ying Chen [1,4], Lin-Yi Gu [4] and Shi-Lun Li [4]

[1] Ocean College, Zhejiang University, Hangzhou 310058, China;
E-Mails: arwang@zju.edu.cn (J.-W.C.); ychen@zju.edu.cn (Y.C.)

[2] Department of Mechanical Engineering, University of Hawaii at Manoa, Honolulu, HI 96822, USA; E-Mail: bsb@hawaii.edu

[3] Department of Ocean Engineering, Hangzhou Dianzi University, Hangzhou 310018, China

[4] State Key Laboratory of Fluid Power Transmission and Control, Zhejiang University, Hangzhou 310027, China; E-Mails: lygu@zju.edu.cn (L.-Y.G.); lsl@zju.edu.cn (S.-L.L.)

* Author to whom correspondence should be addressed; E-Mail: wayfan@163.com; Tel.: +86-571-8820-8890; Fax: +86-571-8820-8891.

Received: 27 March 2013; in revised form: 29 May 2013 / Accepted: 24 June 2013 / Published: 9 July 2013

Abstract: A corer, which can obtain long *in situ* pressure-retained sediments of up to 30 m core containing gas hydrates, has been applied in the South China Sea (SCS) dozens of times. The corer presented in this paper is a convenient, efficient and economical long *in situ* pressure-retained coring and research tool for submarine sediments, that can applied to completely cope with all sediments close to the seafloor ranging from shallow waters to the deep sea depths of 6000 m. This article mainly presents the overall structure, working principles, key pressure-retained components, coring mechanism, sea trials and outlook of the corer. The analyses found that the coring ability was affected by formation characteristics, the outer diameter of the core barrels and inner diameter of the core liners, the shapes of the cutter and the dead weight of the corer. This study can provide the practical basis for the structural optimization of this type of corer and designs for corers with greater penetrability. Sea trials showed that the developed corer presented in this paper can support the *in situ* pressure of the seafloor sediment core, which is an improvement over the conventional piston corer.

Keywords: gas hydrate corer; *in situ* pressure-retained corer; mechanism of coring; long coring; gravity-piston; key pressure-retained structure

1. Introduction

Gas hydrates, ice-like crystalline solids containing a high concentration of methane, have attracted world-wide attention because they have been identified as a potential type of clean alternative energy [1]. Diffusion and seepage gas hydrates are the two types of submarine natural gas hydrates studied today. Diffusion gas hydrates are widespread where there are bottom simulating reflectors (BSRs) marking the base of the gas hydrate stability zone on seismic sections, but they occur in deeper locations [2,3]. So far, gas hydrates are obtained mainly based on geophysical exploration and coring drilling. Seepage gas hydrates are highly related to undersea gas seepage without BSR marking. The hydrocarbon gases from deep stratum seep toward the seafloor through the channel, forming natural gas hydrates that deposit on the seafloor under appropriate conditions [4,5]. These types of hydrates are characterized by massive occurrences, shallow burying and high concentrations. Therefore, exposed massive hydrate can be observed on the seafloor. BSRs and blanking zones indicating the existence of gas hydrate in the South China Sea (SCS) have been reported by some researchers [6–8]. McDonell *et al.* [7] demonstrated that the Pratas Islands are the most promising area in the northern SCS for the occurrence of gas hydrates, from the tectonic and sedimentary perspectives.

The best method for obtaining gas-hydrate-bearing sediment samples is *in situ*, as this, keeps their submarine features, including stratum configuration, composition, salinity, pressure, temperature and microorganisms, intact. Marine gas hydrates are sensitive to salinity, pressure and temperature [9,10]. Only with this methodology can the benefits of visualization research be obtained on *in situ* sediments containing natural gas hydrate, analyses of the formation of the sediment, porosity, permeability and saturation of the core as well as of the biological living environment are objective and scientific. Due to the unique physical properties of natural gas hydrates, when the core is lifted up to the sea surface through conventional non-pressure-retained coring, natural gas hydrates will largely or completely decompose due to change in temperature and pressure.

As for the pressure-retained coring technology, an attempt to sample sediment with a pressure corer was partially successful during the 164th cruise of the International Ocean Drilling Program (IODP) in 1995 [11]. The type and service conditions of major pressure-retained corers in use are shown in Table 1. However, it is still difficult to gain a single columnar pressure-retained core with a length greater than 3 m. To solve this problem, this paper presents a developed gravity-piston corer that can obtain long pressure-retained *in situ* sediment core, with the addition of sealed and pressure-retained structures.

This paper is organized as follows: first, it presents a long pressure-retained corer structure, the key developed structure, and especially the pressure-retained structure compared to the gravity-piston corer is described. Then, an empirical model for the prediction of the corer length is proposed. Next, sea trial results and analysis are given. Finally, the relationships between geometry, mass and lithological specifics are discussed; some conclusions are summarized and suggestions are offered for future studies of pressure-retained core transfer.

Table 1. Current service conditions of major pressure-retained corers.

Types	DSDP-PCB	ODP-PCS	HYACINTH-FPC	HYACINTH-HRC	Japan-PTCS
Technical parameters	Max. 6 m coring length; 57.8 mm coring diameter; Max. pressure ≤ 35 Mpa	Max. 0.86 m coring length; 42 mm coring diameter; Max. pressure ≤ 70 Mpa	Max. 1 m coring length; 58 mm coring diameter; Max. pressure ≤ 25 Mpa; non-lithological sediment	Max. 1m coring length; 50 mm coring diameter; Max. pressure ≤ 25 Mpa; non-lithological sediment	Max. 3 m coring length; 66 mm coring diameter; Max. pressure ≤ 30 Mpa
Pressure-retained methods	ball valve; high pressure nitrogen	ball valve/accumuzlator	A piston seal and a flap seal/accumulator	the piston seal and a flap seal/accumulator	ball valve
Temperature-retained methods	Not active	Not active	Not active	Not active	adiabatic and thermoelectric coring liners
Post Treatment	Pressure/temperature	No	V-MSCL	V-MSCL	Pressure/temperature
Coring History	DSDP 42/62/76	ODP 124/139/141/146/196	ODP 194/201/204 IODP 311 India-HGHP-1 China-GMGS-1 Korea-UBGH1	ODP 194/201/204 IODP 311 India-HGHP-1	Mackenzie Delta/ Kashiwazaki field and "Nankai Trough" well

Notes: V-MSCL = A vertical multi-scanning device including magnetic susceptibility, conductivity, P-wave velocity and gamma ray (by GEOTEK Ltd., Northants, UK).

2. A Long Pressure-Retained Corer

2.1. System Components

As shown in Figure 1, a corer consists of a core "*flow in*" unit, a *release* unit, a *core-sealing* unit, a *mud-blocking* unit and other *measuring* units. The core "*flow in*" unit is composed of a core head, including the pilot frame, lead weight and accumulators, a cutter, a piston, a catcher, core barrels, barrel joints and core liners, all of which are designed to penetrate sediments and obtain a columnar core. The *release* unit is mainly composed of a balance beam, a counterweight, a releasing hook, a releasing wire and a holder, and the hook is designed to release the counterweight when the corer comes close to the seafloor. The *coring sealing* unit is composed of a cutter, a complete set of barrels including barrel joints, a pressure chamber, a flap valve and two accumulators, which primarily function to keep the pressure of the coring in-situ. The lower *mud-blocking* unit is mainly composed of a mudflap, a mud scraper ring, four sliding copper bushings and two *water-flushing* tubes. The *measuring* unit is composed of a pressure gauge, two check valves, a gas collection tank and a data logger of the core attitude including a gravity accelerator, a water level sensor and a data storage unit from which data can be stored or monitored in real time.

2.2. Principles of Operation

Compared to a gravity-piston corer, the developed long gravity-piston corer presented in this paper makes the pressure chamber seal the cutter. Its working principles are shown in Figure 2. The operation of this corer can be divided into seven stages. In the *descent* stage (Figure 2a), the corer descends to 0–3 m above the seafloor, where the counterweight touches the sea floor first, suddenly releasing the vertical tension on the counterweight wire; this allows the beam to rise in the *releasing* stage (Figure 2b). Then the hook is triggered, and the releasing wire slides down from it, allowing the

corer to fall to the seafloor with its dead weight in the *fall* stage (Figure 2c). An extra 0–3 m cable is connected to the piston in reserve so that the piston can theoretically remain on the sea floor with the descending winch wire before the corer penetrates the sediment. Next, the corer will bores deeper into the sediment while the piston remains stationary relative to the seafloor, which moves upward relative to the cutter; thus, the space between the cutter and the piston end lengthens during the *penetration* stage (Figure 2d). Then the sediment below the cutter *flows directly into* the cutter and the core liners when the corer falls freely. At the same time, a slipping seal condition exists between the piston and the core liners, allowing the creation of a vacuum between the bottom of the piston and the sediment surface; this makes more sediment core easily flow into the liners, as it helps overcome the frictional forces between the cored sediment and the internal wall of the core liner. Thus, a much longer core may be obtained with this piston-corer compared to gravity corers, due to the piston located inside the core liners. It takes five to eight s to penetrate the sediment and finish the "*flow in*" process. Then the tension of the winch wire suddenly drops when monitoring the tension gauge, so the winch stops to lower the wire between 10 s and 2 min. When the piston wire is lifted up, the piston is raised back to the upper section of the barrel; then it radially pushes four spring bolts mounted on the top of the pressure chamber causing the core head to suddenly drop down with the pressure chamber by the dead weight. This allows the entire set of barrels to move up along the upper center bores of the pressure chamber in the *core-head free* stage (Figure 2e). If the piston wire is continuously pulled back, allowing the cutter to access the half-moon mudflap at the bottom of the pressure chamber, the core will be cut by the mudflap by the force of a spring. As the barrels continue to slide up, their outer surfaces will be touch the inner surfaces of the sliding copper bushings which are used to keep the barrels moving perpendicular to the bottom surfaces of the four slip blocks. Because the outer diameter of the cutter is larger than that of the core barrels, when the cutter touches the sliding copper bushings, the copper bushings are pushed up and out radially so that the outer surface of the cutter comes in complete contact with the sliding copper bushings and can move upward. When the cutter passes through the flap valve of the pressure chamber, the door returns to its normal position by the spring's torsion and self-gravity, and the cutter is completely sealed in the center bore at the upper end of the pressure chamber in the *retraction and lift* stage (Figure 2f) and the *lift* stage (Figure 2g). The pressure-retained coring process of the submarine hydrate sample is then complete. In addition, thermal insulation materials are used as a coating inside and outside the chamber, and there are polycarbonate core liners in the barrels, all of which can slow down the temperature changes that occur during the lifting of the core from the seafloor to the deck. When the corer is taken back on board, the gas collection is reduced and decompressed, and the coring is cut into segments, which are then transferred into refrigeration storage on board.

Figure 1. Components of the long pressure-retained gravity-piston corer.

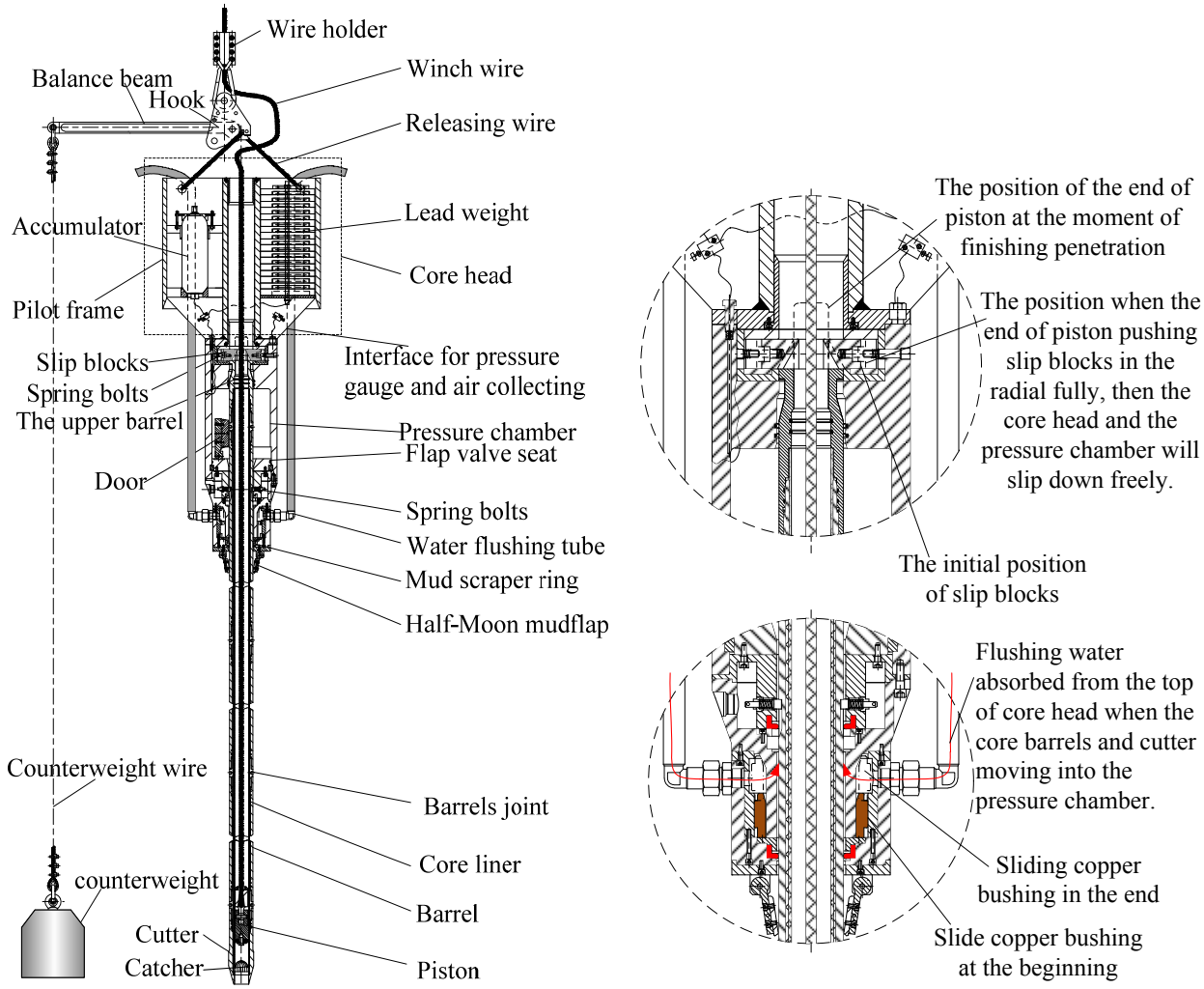

Figure 2. Operation of the long pressure-retained gravity-piston corer: (**a**) descent; (**b**) releasing; (**c**) fall; (**d**) penetration; (**e**) core head and pressure chamber free; (**f**) retraction and initial lift; and (**g**) lift.

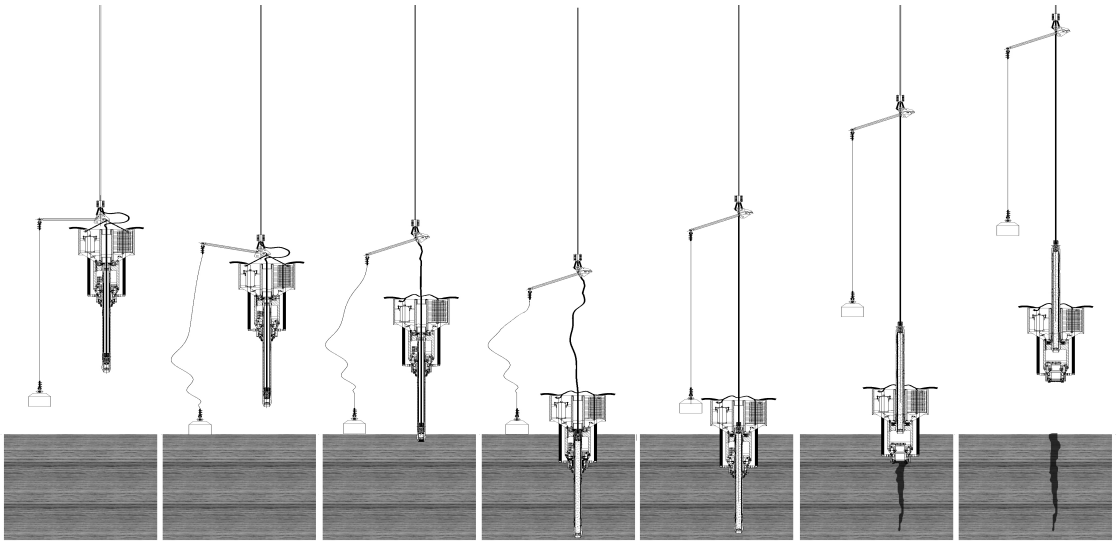

(**a**) (**b**) (**c**) (**d**) (**e**) (**f**) (**g**)

2.3. The Key Structure for Coring with Retained Pressure

The pressure-retained corer designed in this study is an improvement over the gravity-piston corer; it has the same function as the gravity-piston corer but has the addition of a pressure-retained function during the coring process. The key question is how to seal the core cutter; currently, it is sealed only by means of mechanical triggers. The pressure-retained corer's major structural improvements over gravity-piston corer are listed below.

(1) The outer diameter of the screw-threaded barrel joint is the same as that of the barrels, allowing the whole set of core barrels to slip freely upward along the center hole of the pressure chamber, while gravity-piston corers normally have coupling sleeves with a little larger outer diameter; However the piston corer presented in this paper has a cutter with a larger outer diameter than that of the barrels; this creates a seal between the cutter and the pressure chamber at the bulge of the cutter.

(2) The core head and the pressure chamber are assembled integrally, acting as the dead weight to penetrate. The core head is made of the pilot frame, lead weight and two accumulators.

(3) The four major sealing structures that retain pressure on the core include the seal between the piston and the upper section of the core barrels (Figure 3a), the seal between the coring cutter and the upper opening of the pressure chamber, the seal between the door and the flap valve seat (Figure 3b), the seal between the screw-threaded coupling sleeve and both sides of two barrels (Figure 3c), and two accumulators mounted in the pilot frame, the accumulators are used to compensate for the change of volume due to the change of pressure between the inside and the outside of the barrels and the pressure chamber when the corer is pulled up on board.

Figure 3. Four key sealing structures: (**a**) When the piston is pulled up by the winch wire to the end of the upper section of the core barrels, there are two O-rings to keep the seawater in the core from leaking out; (**b**) There are two seals, and when the core cutter is lifted up to the end of the center hole, there are two O-rings in case of leakage. When the door is turned to the conical opening of the flap valve seat, there is also an O-ring between them; and (**c**) at both sides of the screw-threaded coupling sleeve, there are two smooth guide pipe segments, the two O-rings seal the smooth guide pipe segments and the core barrels.

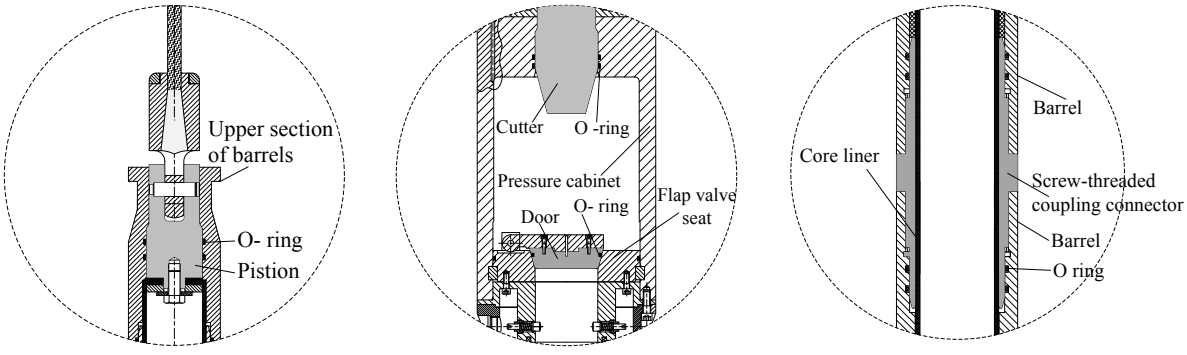

(**a**) (**b**) (**c**)

(4) Two water-flushing tubes are mounted on both sides of the mud flap because there was a failure to maintain pressure without these tubes during the first sea trial. It was found that the door of the flap valve was not easy to fully close with mud on the conical surface of the flap valve seat. Furthermore, when the core head and the pressure chamber would slip down along the core barrels and penetrate the mud near the seabed, there would be an enclosed space at the bottom of the pressure chamber. When the winch wire lifts up the core barrels, the sediment is absorbed under the cutter and flows into the mud flap and the pressure chamber like a syringe pump. After the flushing tubes were mounted, the flushing water could be absorbed easily through the tubes from the top of the core head and would compensates for the increasing space between the cutter and the sediment below; meanwhile, the flushing water could clean the mud on the conical surface of the flap valve seat (Figure 4). Although the half-moon flap can block the mud flowing up into the pressure chamber, sometimes the half-moon flap would not work when the corer sinks into harder sediment stratum. There were more chances to succeed after mounting the unit after the first sea trial.

Figure 4. Water-flushing structure: (**a**) When the core barrel lifts up, the slide copper bushings are pushed upward and then pushed radially; then, the half-moon mudflap will close; (**b**) When the mudflap is closing and the core barrels are being lifted up, there is lower pressure, and the water at the top of the core head is absorbed into the space between the cutter and the mudflap through the flushing tubes; therefore the pressure chamber and the core head are not lifted; and (**c**) when the core barrels enter the pressure chamber, the door closes by the spring tension. The flushing water cleans the conical surface of the flap valve seat and the surface of the door; this is important to establish the seal.

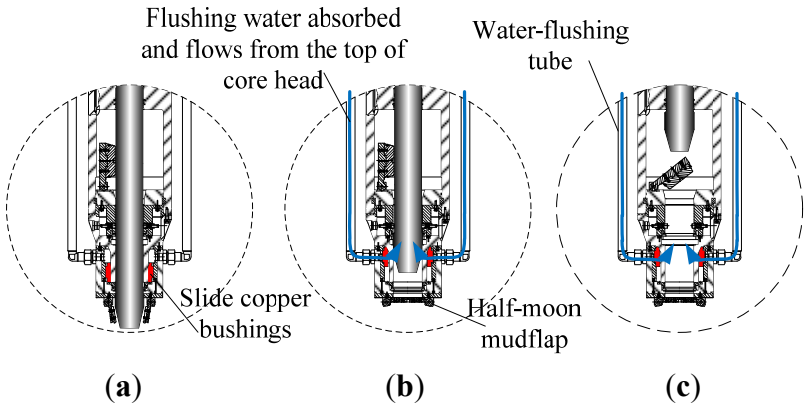

(5) In the corer's descending process, the barrels are hooked by four equally spaced spring bolts in the *mud-blocking* unit (Figure 5). When the releasing wire is removed, the core head and the pressure chamber with the *mud-blocking* unit lose their bearing force by the four spring bolts; then they slip down along the slopes in the four grooves on one of the barrels and push the spring bolts radially. Thus, the dead weight of the core head and the pressure chamber with the *mud-blocking* unit act on the top surface of upper barrels (Figure 6a) and force the barrels to penetrate the sediment and make the core "*flow into*" the core liners. When the piston and the barrels are raised up, the four spring bolts mounted on the upper pressure chamber (Figure 6b) are pushed radially by the end of the piston; at that time, the end of the upper barrel acts

directly upon the slopes of the four stiff slip blocks of the spring bolts, which are made of quenched-and-tempered stainless steel-3Cr13. Due to the dead weight of the core head, the pressure chamber and the mud-blocking unit, the four slip blocks are forced to move along the horizontal grooves (Figure 6c). The barrels are raised along with the piston (Figure 6d), and thus the core head and the pressure chamber freely slip down along the outer surface of the barrels.

Figure 5. Structure of the four springs bolts hooking the barrels.

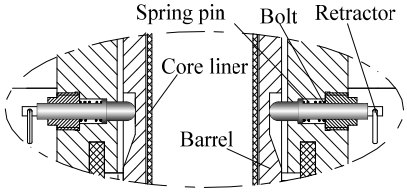

Figure 6. Moving sequence of the four spring bolts and piston: (**a**) The upper section of the piston touches the conical surfaces of the slip blocks of the spring bolts; (**b**) The spatial mounted four spring bolts are forced to move radially by the top end of the piston; (**c**) The four spring bolts are forced to move continuously by the dead weight of the core head, the pressure chamber and the *mud-blocking* unit; and (**d**) the whole barrels pass freely through the four spring bolts.

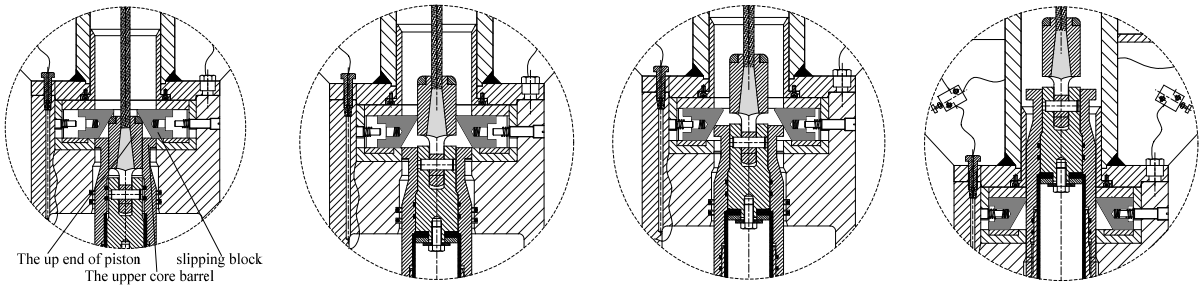

3. Mechanism of the Core

The coring mechanism of the gravity-piston corer can be analyzed based on the concept of the soil plug effect for open-ended piles in geotechnical research. By analyzing the process of the corer penetrating the soil (the force is shown in Figure 7), it is determined that the forces act upon the corer as shown in Equation (1); this influences the corer's penetration as follows: (a) G the dead weight of the corer; (b) F_i the contact resistance between the inner surface of the core liners and the soil; (c) F_o the contact resistance between the outer surface of the barrels and the soil; (d) F_c the contact resistance between the outer surface of the cutter and the soil mass; (e) F_B the buoyancy of the corer in the water; and (f) F_D the water drags force on this corer. To calculate the penetration force of the corer, Smith [12] used the lumped-mass model, which holds that, if the corer penetrates quickly into the sediment, assuming that the original properties of the sediment are not broken, the sediment bears the instantaneous load while it causes immediate deformation and obtains geostatic pressure equal to or greater than that in the original stratum. This mechanical model should increase the mass stiffness as the loading force acting on the sediment increases.

$$\Delta F = G - \left(F_i + F_o + F_c + F_B + F_D\right) \tag{1}$$

Figure 7. Diagram of all forces on the corer.

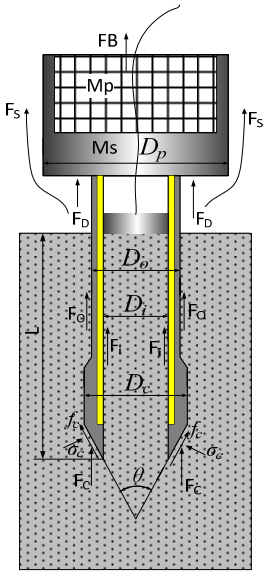

3.1. Inner Surface Friction Force

According to geomechanics, the shear strength of soil-τ, is given analytically by the following straight-line equation, known as Coulomb's shear strength equation [13]:

$$\tau = \sigma \tan\varphi + c \ (\text{kg/cm}^2) \tag{2}$$

where the intercept c, is defined as the cohesion of the soil; φ = the angle of the internal friction of the soil; and σ = the effective normal stress on the rupture plane. In fact, to get the general geological features of the working region, current seabed sediment coring is generally based on experience, existing submarine geological data and subbottom profile information. Therefore, this study provides some empirical formulas to calculate the submarine shear strength. Silva *et al.* [14] expressed the undrained shear strength of sea bottom mud, which varies linearly with depth (<40 m), in the vane shear test. The relationship between shear strength and depth is:

$$C_u(h) = 1 + 1.3h \ \text{kPa} \tag{3}$$

If $h = 0$, the shear strength of the interface between sea mud and seawater is 0; if h is 15 m, the shear strength is 20 kPa. Then, the static resistance-R_s is calculated, as shown in Equation (4):

$$R_s = 1000\pi D_i \int_0^l \alpha_i \left(1 + 1.3l\right) dl \tag{4}$$

where D_i is the inner diameter of the core liner; α_i is the coefficient of friction; and l is the actual length of the core. Thus, the internal friction of core liner-F_i, which is the same as the dynamic soil resistance can be obtained by Smith's wave equation model [12], as shown in Equation (5):

$$F_i = 1000\left(1 + J_s v\right)\pi D_i \int_0^l \alpha_i \left(1 + 1.3l\right) dl \tag{5}$$

where v is the penetration velocity; and J_s is the viscous damping factor of the side wall surface. According to the operation principle of the piston corer, the length of the core is equal to the penetration depth-L of the corer under ideal conditions.

According to Smith [15], for clay, the pile-soil coefficient of friction (called an adhesion factor) has been found to vary from 0.3 to 0.6. Paik and Lee [16] indicated that, when an open-ended pile was inserted into unconsolidated saturated soil, the vertical stress of the core in the tube maximized at its end of the pile while it decreased quickly to 0 upward along the core. Skinner and McCave [17] indicated that the internal friction of the bottom upward within 1.5 m was calculated only if the plug occurred. However, the sediment smearing dissipated in the gravity-piston corer due to the working features of the piston corer under ideal conditions. Therefore, internal friction is still calculated by total friction acting upon the inner surface of the core liner within 1 to 1/3 of the full penetration depth.

3.2. Outer Surface Friction Force

As an intact process of the corer penetrating the soil, external friction is also an important consideration. By analyzing the structural features of the end of the cutter, the coring has basically no sideways extrusion on the internal surface of the cutter, while the bottom sediments are extruded sideways by the conical surface of the cutter; this results in rapid drainage, which has a direct impact on the increase in the shear strength of the very thin layer of sediment that touches the outer surface of the core barrels. Like the equation for internal friction, the equation for external friction is obtained as follows:

$$F_o = 1000\left(1 + J_s v\right)\pi D_o \int_0^L \alpha_o k\left(1 + 1.3L\right)dL \tag{6}$$

where L is the penetration depth of the barrels into the bottom sediment; α_o is the coefficient of friction for the barrels outer surface; and k is the enhancement factor of the shear strength of the extruded sediment on the outer wall surface of the coring barrels, with the k value of 1.1 used in this study.

3.3. Resistance of the Cutter

The vertical resistance-F_c given by sediments at the end of the cutter is:

$$F_c = \left(1 + J_c v\right)\left(\sigma_c A_c \sin\left(\frac{\theta}{2}\right) + \alpha_c \sigma_c A_c cos\left(\frac{\theta}{2}\right)\right) \tag{7}$$

where J_c is the viscous damping factor of the cutter's inclined surface; σ_c is the effective normal foundation bearing stress; A_c is the conical surface area of the cutter; and θ is the angle of the cutter cone.

It can be seen that the equation has minimal resistance on the cutter head under the condition that the cutter's own materials and structure meet the permissive compressive strength. Thus, $\frac{dF_c}{d\theta} = 0$, and $\cos\left(\frac{\theta}{2}\right) - \alpha_c \sin\left(\frac{\theta}{2}\right) = 0$.

Thus, $\theta = 2arccta\left(\alpha_c\right)$. If $\alpha_c = 0.3$, then θ = 16.692°. According to the permissive condition of the strength of the cutter itself, in this study, its angles are designed to be 30°, and $A_c = \frac{\pi D_c\left(D_c - D_i\right)}{4\sin\left(\frac{\theta}{2}\right)}$, then:

$$F_c = \frac{\pi}{4}(1 + J_c v)\sigma_c D_c (D_c - D_i)\left(1 + \alpha_c \cot\left(\frac{\theta}{2}\right)\right) \tag{8}$$

where D_c is the outer diameter of the cutter; while $\sigma_c = \tau_c / \alpha_c$; τ_c is the undrained shear strength of the soil near the cutter's inclined surface. In this study, all shear strengths on the conical surface of the cutter in contact with sediment are the same. Then $\tau_c = k(1 + 1.3L)$, $\sigma_c = \frac{k}{\alpha_c}(1 + 1.3L)$, and finally:

$$F_c = 1000\frac{\pi k}{4\alpha_c}(1 + J_c v)(1 + 1.3L)D_c (D_c - D_i)\left(1 + \alpha_c \cot\left(\frac{\theta}{2}\right)\right) \tag{9}$$

3.4. The Underwater Lead Weight of the Corer

The corer mainly consists of high strength, 17-4PH stainless steel, and cast lead, thus W —the dead weight is equal to:

$$W = (M_s + M_P)g \tag{10}$$

where, M_s is the total mass of the components excluding the lead weight; M_P is the mass of lead weight; ρ_w is the water density; and g is the acceleration of gravity. Thus the buoyancy F_B acting on the corer is as follows:

$$F_B = \rho_w\left(\frac{M_s}{\rho_s} + \frac{M_P}{\rho_P}\right)g \tag{11}$$

Then W_w —the underwater dead weight of the corer is:

$$W_w = W - F_B = M_s g\left(1 - \frac{\rho_w}{\rho_s}\right) + M_p g\left(1 - \frac{\rho_w}{\rho_P}\right) \tag{12}$$

3.5. The Drag Force in Water

While vertically penetrating the corer, if it is accelerating against the seawater, its resistance is chiefly from the upstream resistance, and its side friction is very low, so the side friction is negligible in this study. If all the lead weight is mounted on the core head, then the area of the upstream face is $\frac{\pi}{4}(D_p^2 - D_o^2)$. Therefore, the upstream resistance-F_d is obtained by the following equation [18]:

$$F_d = \frac{1}{2}\rho_w v^2 \frac{\pi}{4}(D_p^2 - D_o^2)C_d = \frac{2.55\pi}{Re}\rho_w v^2 (D_p^2 - D_o^2) \tag{13}$$

where R_e is the Reynolds number; D_p is the outer diameter of the core head; v is the penetrating velocity of the corer, and:

$$R_e = \rho_w v D_p / \mu_w \tag{14}$$

Then:

$$F_d = 2.55\pi v D_p \mu_w \tag{15}$$

where μ_w is the viscosity of the water *in situ*.

3.6. Penetration Control Equation

The final penetration equation, as shown in Equation (16) can be obtained by substituting Equations (5–7) and (9) for Equation (1):

$$\begin{aligned}(M_s+M_P)a=&\left(M_sg\left(1-\frac{\rho_w}{\rho_s}\right)+M_pg\left(1-\frac{\rho_w}{\rho_p}\right)\right)\\&-\left(1000\left(1+J_sv\right)\pi\alpha_i\left(D_i\int_0^L\left(1+1.3L\right)dL+D_o\int_0^Lk\left(1+1.3L\right)dL\right)\right)\\&-250\left(1+J_cv\right)\frac{k\pi}{\alpha_c}\left(1+1.3L\right)D_o\left(D_o-D_i\right)\left(1+\alpha_c\cot\left(\frac{\theta}{2}\right)\right)-2.55\pi vD_p\mu_w\end{aligned}\tag{16}$$

where a is the acceleration of the corer.

3.7. The Uplift Force of the Corer

Murthy [19] has produced force analyses on tension piles, uplift piles and anchor piles. The forces of these piles are mainly from geostatic pressures and skin frictions. The corer experiences a very short cycle from penetration and coring to recovery and then is lifted back up within 2 min. Therefore, it can be determined that the sediment extruded around the barrels has not yet consolidated, and the recovery process is still treated as a spring-damper system. Thus the uplift force F_l is:

$$F_l=W_w+1000\left(1+J_sV_w\right)\left(\pi D_o\int_0^Lk\alpha_0\left(1+1.3L\right)dL\right)=W_w+1000\pi k\alpha_0D_o\left(1+J_sV_w\right)\left(L+\frac{1.3}{2}L^2\right)\tag{17}$$

where W_w is the velocity of the winch wire (unchanged) and thus the max uplift force can be calculated from Equation (17) in the empirical formula.

The uplift force F_l will get maximum value in the moment of uplift, so the tension of the winch wire must be higher than the force F_l; then the corer can be easily uplifted.

4. Results and Discussion

4.1. Sea Trials

From 2006 to 2011, several experimental investigations were carried out on the Guangzhou marine geological research vessel (R/V Haiyang 4 and R/V Haiyang 6). Experimental data are shown in Table 2. In 2006, the first corer (1st LPC) failed to obtain core and maintain *in situ* pressure for the core many times. However, in 2011, the developed gravity-piston corer presented in this paper is a 30 m long corer (2nd LPC), obtaining the core at each penetration. But only 3/5 of penetrations, the core had maintained the *in situ* pressure which was better than that of the first corer. The most important improvement over the first corer was the addition of two water-flushing tubes; this reduced failures due to the door of the flap valve being blocked by the bottom mud taken in when retracting the core barrels. In 2011, the length of this core barrels reached 30 m; however, only 22 m long corer barrels were used due to the limited dimension of the vessel deck. To date, the best records are that of a 14.5 m long pressure-retained sediment core at 1600 m water depth and an 18.5 m long core without *in situ* pressure. Figure 8 shows the long pressure-retained corer operating onboard during a sea trial in 2011.

Table 2. Sea trial results for a long pressure-retained corer.

Site Name	Date	Location	L_d (m)	P_c (MPa)	L_c (cm)	M_c (kg)	Specifics of Corer
387PC	15 August 2006	Paracel Islands	1400	0	900	1300	OD 105 mm; ID 75 mm
373PC	16 August 2006	Paracel Islands	1400	14	900	1300	OD 105 mm; ID 75 mm
DSH-1	19 August 2006	Pratas Islands	3150	0	160	1300	OD 105 mm; ID 75 mm
DSH-1	19 August 2006	Pratas Islands	3050	0	0	1300	OD 105 mm; ID 75 mm
DSH-1	20 August 2006	Pratas Islands	3050	0	753	1300	OD 105 mm; ID 75 mm
DSH-1A	20 August 2006	Pratas Islands	3050	30	658	1300	OD 105 mm; ID 75 mm
DSH-1C-1	22 August 2006	Pratas Islands	3050	32	659	1300	OD 105 mm; ID 75 mm
DSH-1C-2	22 August 2006	Pratas Islands	3050	0	624	1500	OD 105 mm; ID 75 mm
DSH-7	23 August 2006	Pratas Islands	3050	32	957	1500	OD 105 mm; ID 75 mm
DSH-9	23 August 2006	Pratas Islands	3050	34	957	1500	OD 105 mm; ID 75 mm
DSH-1D	24 August 2006	Pratas Islands	3050	0	963	1500	OD 105 mm; ID 75 mm
DSH-13	24 August 2006	Pratas Islands	3050	0	884	1500	OD 105 mm; ID 75 mm
Jiulong Reef	25 August 2006	Jiulong Reef	760	9	20	1500	OD 105 mm; ID 75 mm
Jiulong Reef	25 August 2006	Jiulong Reef	760	2	500	1500	OD 105 mm; ID 75 mm
BZ888	9 May 2006	115°26.0922' E/19°18.8040' N	2470	0	944	1300	OD 105 mm; ID 75 mm
BZ526PC	26 May 2006	111°47.0962' E/17°45.1193' N	1940	20	915	1300	OD 105 mm; ID 75 mm
DHCL12	17 April 2011	118°47.4258' E/22°00.8804' N	1023	9.5	12.1	1800	OD 112 mm; ID 90 mm
973-4	22 April 2011	118°49.0818' E/21°54.3247' N	1600	16.5	14.5	2500	OD 112 mm; ID 90 mm
DHCL13	25 April 2011	118°44.6179' E/22°01.5884' N	850	8.8	9.7	2500	OD 112 mm; ID 90 mm
9735	26 April 2011	119°11.0066' E/21°18.5586' N	3050	0	9.65	2500	OD 112 mm; ID 90 mm
PPC1	20 May 2011	116°53.4988' E/17°51.9969' N	4000	2	18.5	2500	OD 112 mm; ID 90 mm

Notes: L_d = water depth; P_c = coring pressure; L_c = length of the coring; M_c = the total weight of the corer.

Figure 8. Photographs of a 2011 sea trial. (**a**) The corer is ready to descend into the sea from the corer bracket; (**b**) After being lifted up from the seafloor, the corer is put into the corer bracket again and then lifted to the vessel deck along with the bracket; (**c**) When the corer is fixed to the bracket on the deck, the pressure gauge shows the *in situ* pressure; (**d**) While decreasing the core pressure to the current barometric pressure, an air collector is used onboard to collect the gas in the core; and (**e**) then the barrels are dismantled, and the whole core liners with the core in it are split into segments after releasing the core pressure.

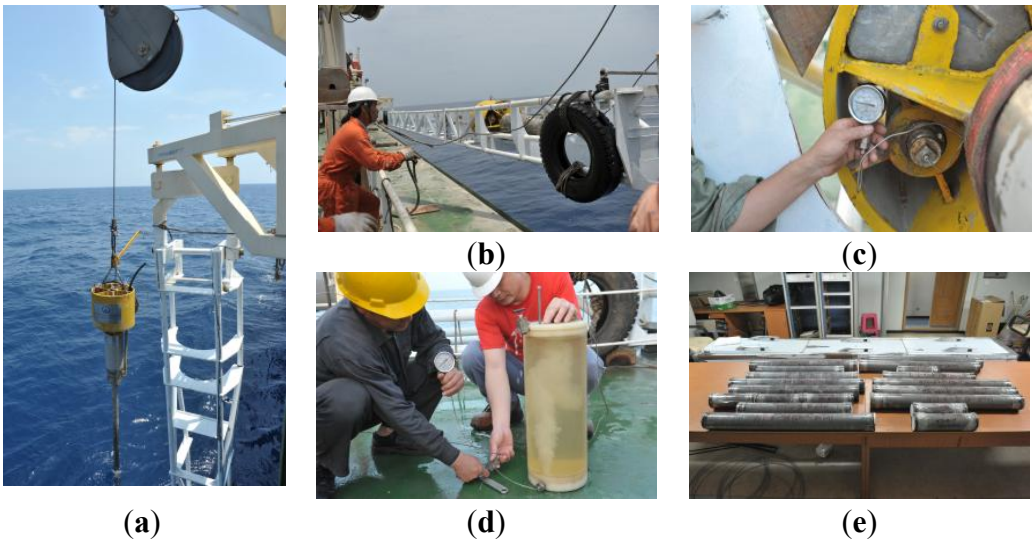

(**a**) (**b**) (**c**) (**d**) (**e**)

4.2. Discussion

4.2.1. Influence of Lead Weight on Coring Depth

Lead weight plays a critical role in penetration depth. When the Woods Hole Oceanographic Institution (WHOI) obtained a 45 m long core sample in 2008, its lead weight was about 15 t [20]. The MDII Calypso Piston Corer on board the R/V Marion Dufresne II obtained a 57.34 m long core sample with 6 t of dead weight by a piston corer in Antarctic waters in 2003 [21]. In 2012, the State Key Laboratory of Marine Geology at Tongji University and the French Climate and Environmental Science Laboratory carried on a project called CIRCulation in East Asian area-CIRCEA, that is the cruise MD190, the cores were obtained between 31.9 and 50.8 m long with a 4 t lead weight on the core head by the Calypso piston corer [22]. This study provided a penetration model based on the interaction between the corer and the sediment. The relationship between dead weight and penetration depth is shown in Figure 9. Coring depth varies with the lead weight of the corer such that increasing the lead weight improves penetration. The shear strength of the stratum has been defined in Equation (3), but the actual stratum situation is relatively complex, as shown in Table 2. In 2006, cores at both the 387PC and 383PC sites of the Paracel Islands (1st LPC) were full of core liners due to soft sediments. Therefore, it could be determined that the actual penetration depth of the corer was longer than the length of the coring in the core liner. For the DSH-1-1, DSH-1-2, and DSH-1-3 sites, the core liner only obtained a short core length due to hard sediments in the Pratas Islands waters. Judging by both the DHCL12 and 973-4 sites in 2011 (2nd LPC), the corer penetrated the sea bottom sediment incompletely. The longest sample lengths were obtained by the 1st LPC and the 2nd LPC pressure-retained corers and the WHOI long corer (Cruise KNR195-3, KNR 195-5, KNR 197-3, KNR 197-4, KNR 197-10 and KNR 198-1), all of which were close to or less than the basic theoretical value. Marion MD03-2597 obtained a 57 m long core sample with a Calypso piston corer with about 6 t of lead weight, finding that its sediments were very soft diatomaceous ooze, which improved the coring depth. In 2002, Marion Dufresne Cruise MD-02 investigated the occurrence and distribution of gas hydrates in the shallow subsurface from the upper continental slope of the northern Gulf of Mexico using the giant Calypso piston corer. All cores were less than 40 m still very near the theoretical value. However, the corer had 8 t of lead weight, and, its sediments were present as hardgrounds [23].

Figure 9. Relationship between load weight and penetration depth.

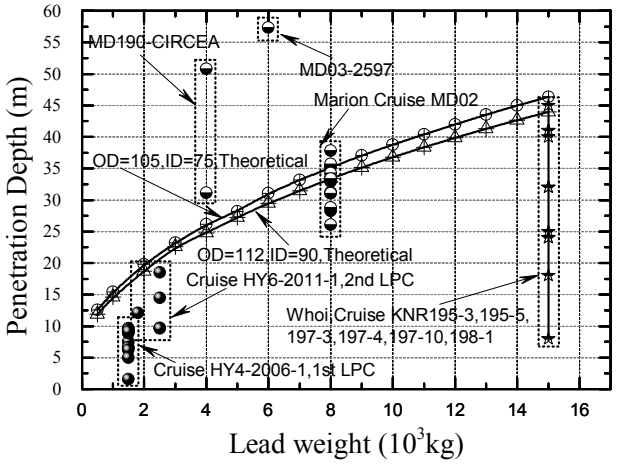

4.2.2. Analysis of the Coring Process

Figure 10 shows curves of a 105 mm OD, a 75 mm ID and a 1.5 t corer whose acceleration, velocity and displacement vary with time. It can be seen that the corer usually finished penetration within about five to eight s. In practice, once the winch wire tension is suddenly removed, the corer will be lifted up within ten s. These curves show that initially, the underwater dead weight of the corer is far greater than the friction resistance between the sidewalls and the sediment or between the corer and the water. Thus, the corer will drop sharply. When the corer is stuck in the sediment, its acceleration will initially decrease and reach the minimum (negative) due to increased frictional resistance. The velocity will rapidly decrease, and the corer may rebound in coring when its velocity first decreases. Figure 11 shows that, if the friction coefficient between the sediment and the sidewall increases, it is not easy for the corer to rebound during penetration. This is more likely to happen to the second coring. This is not benefit to analyze the core in the after treatment in laboratory. Figure 12 shows that the rebound height and the maximum penetration depth of the corer vary with the lead weight but that the rebound amplitude decreases as the lead weight increases.

Figure 10. Variation of the acceleration, velocity and displacement of the corer during penetrating.

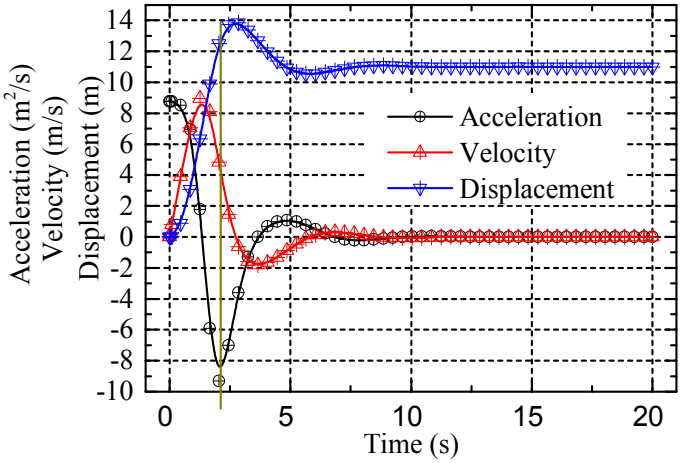

Figure 11. Variations of rebound height *vs.* different lithology viscosity between the barrel and the soil.

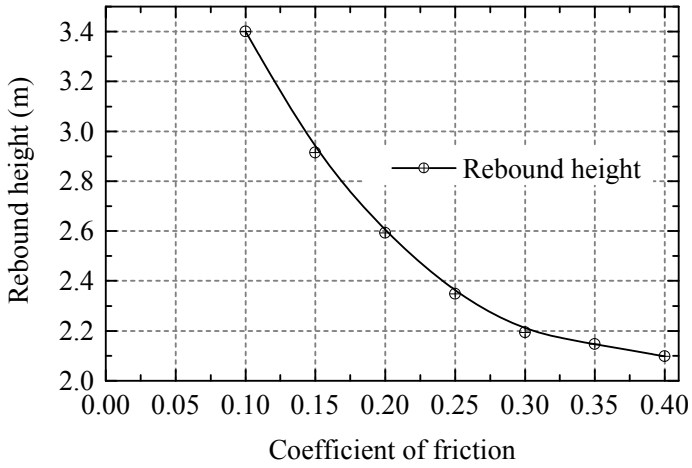

Figure 12. Variations of rebound height and maximum penetration depth *vs.* different lead weight.

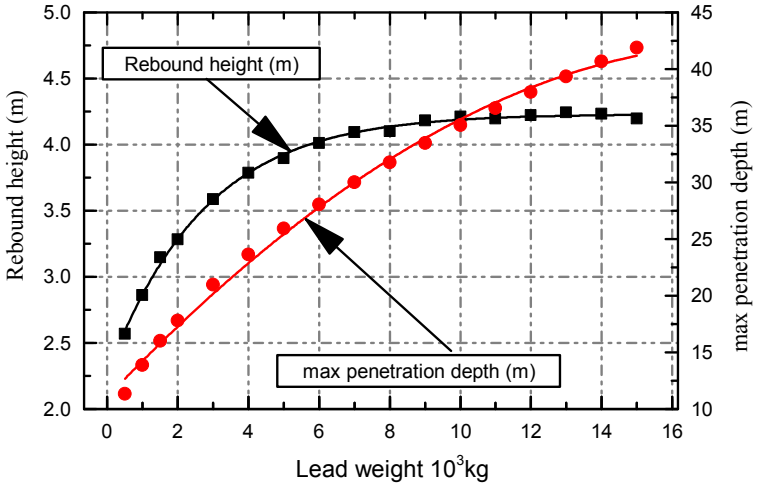

4.2.3. Influence of the Inner Diameter of the Coring Liner

When the inner diameter (ID) of the core liner decreases, the penetration into strata will be subjected to the soil plug effect. The coring length differs with the penetration depth. To analyze this, only the core of the core liner is considered, and the balance equation can be obtained from the weight of plug G_s, side wall friction force τ_s and the bearing resistance at the bottom of cutter P_b, as shown in Figure 13.

Figure 13. Sketch map of forces on the coring.

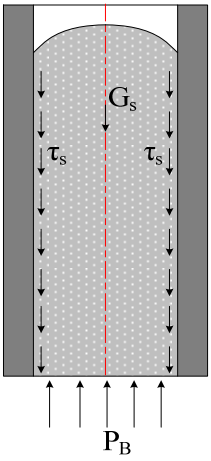

$$G_s + \tau_s = P_b \tag{18}$$

Substitution of the sectional area of the coring and the inner perimeter of the core liner, yields:

$$\frac{\pi}{4} D_i^2 l \gamma_{soil} + \pi D_i l \tau_u = \frac{\pi}{4} P_{tB} D_i^2 \tag{19}$$

where P_{tB} is the bearing stress of the soil; and γ_{soil} is the specific weight, thus:

$$l = P_{tB} / \left(\gamma_s + \frac{4\tau_u}{D_i} \right) \tag{20}$$

When the core "*flown into*" the core liners increases, τ_u will also rise and the side friction in the liners will gradually increases; thus, the longer coring at the very bottom of the core barrels will cause a plugging effect whereby the sediment at the end of the cutter cannot enter the liners. The less γ_s, the longer the core, while the less τ_u, the longer the length of coring l; this shows that soft sediments may easily enter the liners. Based on the undrained, saturated clayey sediments reported by Meyerhof [24], the ultimate bearing capacity of a foundation $P_{tB} = N_c C_\mu A_c$ is obtained, and Meyerhof [25] indicated that N_c could have a value of 9 for undrained saturated clay. Thus, when penetrating the barrels, the bearing capacity of the core sample at the end of the cutter was greater than P_{tB}. Until it was less than and finally equal to P_{tB}, the corer stopped "*flowing in*". It is difficult to maintain the coring quality if the plugging effect occurs in the liners before completely penetrating the sediment. Once this happens, the corer will be unable to continue penetrating, and the recovery process will be apt to absorb the sediment and the water into the core liners so that the piston will be able to be pulled up to the top of the barrels. However, during seal trials, it was found that the liners at the top of the barrels were full of seawater.

4.2.4. Influence of the Outer Diameter of the Coring Barrels on the Coring Process

Figure 14 shows that when the outer diameter (OD) of the coring barrels increases, the penetration depth of the barrels descends nearly linearly. It can also be seen that, at the same OD of the barrels, the core with a smaller ID liner has a longer penetration depth; however, the length of the core obtained depends on Equation (19).

Figure 14. Variations of penetration depth *vs.* different OD.

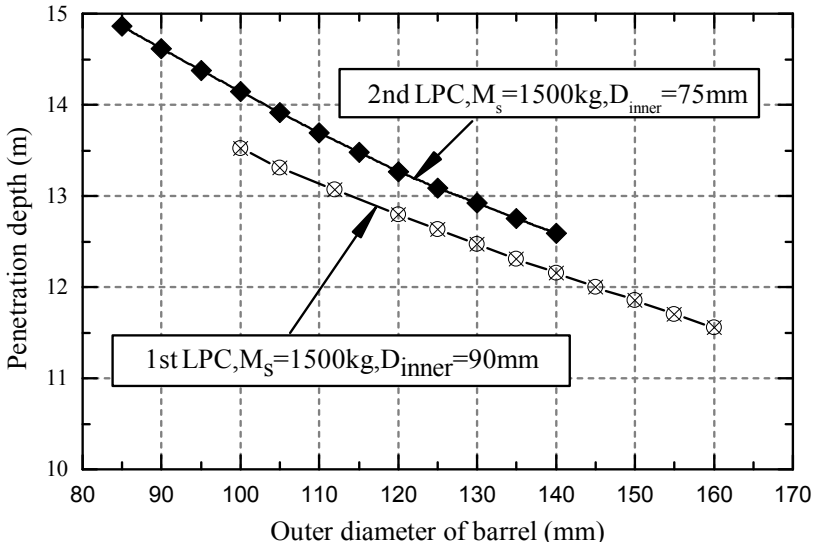

4.2.5. The Release Time is Difficult to Determine in Practice

There is neither an underwater external power supply nor an underwater video system for this gravity-piston corer. When the corer is descending, the counterweight may easily touch the shipboard, leading to the loss of the corer due to a broken wire during free fall. When the corer is descending to the seafloor, unknown strata and topography may cause the corer to be released in advance, or delay

the release so that the corer fails to penetrate vertically at the beginning. The WHOI long corer [20] determined the distance of the corer to the seafloor with an underwater acoustic altimeter, so as to automatically control and release the corer.

4.2.6. The Door of the Flap Valve Makes It Difficult to Ensure Complete Sealing

When the core barrels are uplifted from the seafloor, a great deal of mud and seawater pouring into the pressure chamber will make a certain amount of mud stay on the conical surface of the flap valve seat. If the seal ring does not seal due to failure to pre-compress and deformation of the seal ring, it will result in a failure to retain pressure during the trial. In contrast to the 1st LPC, the design of the two water-flushing tubes greatly improves pressure retention but does not success every time.

5. Outlook

Hugro Technics has developed a pressure-retained transfer device that is compatible with coring tools such as Fugro FPC and FRPC, Aumann HPTC and Hybrid PCS, with a maximum 3.5 m core length [26]. However, it is difficult to directly apply the pressure core analysis and transfer system (PCATs) to the pressure-retained corer presented in this paper. A four-year (2012–2016) core pressure-retained transfer project is being carried out by the Chinese Ministry of Science and Technology. The structure of the corer needed to be improved before that project began.

Acknowledgments

The authors greatly appreciate the support of the captains and crews of the R/V Haiyang 4 (cruise HY4-2006-1) and the R/V Haiyang 6 (cruise HY6-2011-1), as well as excellent technical support from Fanglan Liu, Yan Sheng and Xueqiao Geng of the Guangzhou Marine Geological Survey (GMGS) in China. The authors thank the anonymous reviewers for their detailed and valuable comments which strengthened this manuscript. This study was funded by the China high tech program (No. 2013AA092503 and No. 2006AA09A206) and the program for Zhejiang Leading Team of S&T Innovation (No. 2010R50036).

Conflict of Interest

The authors declare no conflict of interest.

References

1. Makogon, Y.F.; Holditch, S.A.; Makogon, T.Y. Natural gas-hydrates—A potential energy source for the 21st Century. *J. Pet. Sci. Eng.* **2007**, *56*, 14–31.
2. Zhao, J.F.; Yu, T.; Song, Y.C.; Liu, D.; Liu, W.G.; Liu, Y.; Yang, M.J.; Ruan, X.K.; Li, Y.H. Numerical simulation of gas production from hydrate deposits using a single vertical well by depressurization in the Qilian Mountain permafrost, Qinghai-Tibet Plateau, China. *Energy* **2013**, *52*, 308–319.
3. Rutherford, S.R.; Williams, R.H. Amplitude-versus-offset variations in gas sands. *Soc. Explor. Geophys.* **1989**, *54*, 680–688.

4. Baristeas, N.; Anka, Z.; di Primio, R.; Rodriguez, J.F.; Marchal, D.; Dominguez, F. Distribution of hydrocarbon leakage indicators in the Malvinas Basin offshore Argentine continental margin. *Mar. Geol.* **2012**, *332–334*, 56–74.
5. Li, L.; Lei, X.H.; Zhang, X.; Sha, Z.B. Gas hydrate and associated free gas in the Dongsha Area of northern South China Sea. *Mar. Pet. Geol.* **2013**, *39*, 92–101.
6. Wu, S.; Zhang, G.; Huang, Y.; Liang, J.; Wong, H.K. Gas hydrate occurrence on the continental slope of the northern South China Sea. *Mar. Pet. Geol.* **2005**, *22*, 403–412.
7. McDonnell, S.L.; Max, M.D.; Cherkis, N.Z.; Czarnecki, M.F. Tectono-sedimentary controls on the likelihood of gas hydrate occurrence near Taiwan. *Mar. Pet. Geol.* **2000**, *17*, 929–936.
8. Shyu, C.T.; Chen, Y.J.; Chiang, S.T.; Liu, C.S. Heat flow measurements over bottom simulating reflectors, offshore southwestern Taiwan. *Terr. Atmos. Ocean Sci.* **2006**, *17*, 845–869.
9. Zhao, J.F.; Cheng, C.X.; Song, Y.C.; Liu, W.G.; Liu, Y.; Xue, K.H.; Zhu, Z.H.; Yang, Z.; Wang, D.Y.; Yang, M.J. Heat transfer analysis of methane hydrate sediment dissociation in a closed reactor by a thermal method. *Energies* **2012**, *5*, 1292–1308.
10. Zhao, J.F.; Yao, L.; Song, Y.C.; Xue, K.H.; Cheng, C.X.; Liu, Y.; Zhang, Y. In situ observations by magnetic resonance imaging for formation and dissociation of tetrahydrofuran hydrate in porous media. *Magn. Reson. Imaging* 2**011**, *29*, 281–288.
11. Dickens, G.R.; Paull, C.K.; Wallace, P. Direct measurement of in situ methane quantities in a large gas-hydrate reservoir. *Nature* **1997**, *385*, 426–428.
12. Smith, E.A.L. Pile-driving analysis by the wave equation. *Trans. Am. Soc. Civil. Eng.* **1962**, *127*, 1145–1193.
13. Coulomb, C.A. Essai sur uneapplication des règles de maximis et minimis à quelques problèmes de statique, relatifs à l'architecture [in French]. *Mém. Math. Phys*. **1776**, *7*, 343–382.
14. Silva, A.J.; Hollister, C.D.; Laine, E.P.; Beverly, B.E. Geotechnical properties of deep sea sediments: Bermuda Rise. *Mar. Geotech*. **1976**, *1*, 195–232.
15. Smith, G.N.; Smith, I. *Elements of Soil Mechanics*, 8th ed.; Wiley-Blackwell Publishing: Edinburgh, UK, 1998.
16. Paik, K.; Lee, S. Behaviour of soil plugs in open-ended model piles driven into sands. *Mar. Geores. Geotech.* **1993**, *11*, 353–373.
17. Skinner, L.C.; McCave, I. Analysis and modelling of gravity- and piston coring based on soil mechanics. *Mar. Geol.* **2003**, *199*, 181–204.
18. Munson, B.R.; Young, D.F.; OkIIshi, T.H.; Huebsch, W.W. *Fundamentals of fluid mechanics*, 6th ed.; John Wiley & Sons: New York, NY, USA, 1994; Volume 3, pp. 597–598.
19. Murthy, V.N.S. *Geotechnical Engineering: Principles and Practices of Soil Mechanics and Foundation Engineering*; Taylor & Francis: New York, NY, USA, 2002.
20. Curry, W.; Broda, J.; Keigwin, L.; Mountain, G.; Pisias, N. A new long coring system for R/V Knorr. *Eos Trans. Am. Geophys. Union* **2008**, *89*, 142–143.
21. Maddison, E.J.; Pike, J.; Dunbar, R. Seasonally laminated diatom-rich sediments from Dumont d'Urville Trough, East Antarctic Margin: Late-Holocene Neoglacial sea-ice conditions. *Holocene* **2012**, *22*, 857–875.
22. State Key Laboratory of Marine Geology, Tongji University. The joint voyage between China and France in South China Sea [in Chinese]. *Mar. Geol. Quat. Geol.* **2012**, *4*, 106.

23. Chen,Y.F.; Matsumoto, R.; Paull, C.K.; Ussler, W., III; Lorenson, T.; Hart, P.; Winters, W. Methane-derived authigenic carbonates from the northern Gulf of Mexico—MD02 Cruise. *J. Geochem. Explor.* **2007**, *95*, 1–15.
24. Meyerhof, G.G. The ultimate bearing capacity of foundations. *Geotechnique* **1951**, *1*, 301–332.
25. Meyerhof, G.G. Bearing capacity and settlement of pile foundations. *J. Geotech. Geoenviron. Eng.* **1976**, *102*, 197–228.
26. Schultheiss, P.; Holland, M.; Roberts, J.; Huggett, Q.; Druce, M.; Fox, P. PCATs: Pressure Core Analysis and Transfer System. In Proceedings of the 7th International Conference on Gas Hydrates (ICGH 2011), Edinburgh, UK, 17–21 July 2011.